

Azita Mohagheghian¹ / Kobra Ayagh¹ / Kazem Godini² / Mehdi Shirzad-Siboni^{1,3,4}

Using amino-functionalized Fe₃O₄-WO₃ nanoparticles for diazinon removal from synthetic and real water samples in presence of UV irradiation

¹ Department of Environmental Health Engineering, School of Health, Guilan University of Medical Sciences, Rasht, Iran, E-mail: mshirzadsiboni@yahoo.com

² Department of Environmental Health Engineering, School of Health, Hamadan University of Medical Sciences, Hamadan, Iran

³ Department of Environmental Health Engineering, School of Public Health, Iran University of Medical Sciences, Tehran, Iran, E-mail: mshirzadsiboni@yahoo.com

⁴ Research Center of Health and Environment, Guilan University of Medical Sciences, Rasht, Iran, E-mail: mshirzadsiboni@yahoo.com

Abstract:

In this research, photocatalytic degradation of diazinon by amino-functionalized Fe₃O₄-WO₃ nanoparticles under UV irradiation was investigated with variation of pH, nanocatalyst dose, initial diazinon concentration, different purging gases, H₂O₂ concentration, and type of organic compounds. Under optimal conditions: pH=7, [Diazinon]₀= 20 mg.L⁻¹, nanocatalyst dosage= 0.25 g.L⁻¹, H₂O₂= 5 mM, 99.23 % of the insecticide was removed after 120 min. A decrease was observed in the removal efficiency of diazinon in the presence of different purging gases and organic compounds. Based on the three kinetic models developed in this study, it was found that the removal of diazinon followed the first order kinetic. Also, application of the UV/amino-functionalized Fe₃O₄-WO₃ nanoparticles both increased the performance and decreased electric power consumption. However, 86.17 % of diazinon in real water samples was removed under the optimized conditions. Furthermore, the photocatalytic activity was kept after five successive cycles.

Keywords: photocatalysis, diazinon degradation, amino-functionalized Fe₃O₄-WO₃ nanoparticles, synthesis, synthetic and real water, kinetic

DOI: 10.1515/jaots-2016-0153

Received: October 6, 2016; **Revised:** February 9, 2017; **Accepted:** February 25, 2017

1 Introduction

Water pollution is one the major environmental impacts of irregular and wasteful consumption of water [1–4]. Nowadays, huge quantities of different pesticides are used in agricultural and hygienic aspects, which highly contaminate water bodies. Since the majority of organic pesticides are non-degradable and carcinogenic, they are considered as a powerful category of water contaminants. Some health problems related to these substances like immunosuppressive, cytotoxic, mutagenic and endocrine-disrupting impacts have been documented. Huge amounts of effluents containing various pesticides are discharged into the environment before being treated well [5, 6]. It has been claimed that many receiving waters have been polluted by these kinds of substances. The European Economic Community advises that the concentrations of pesticides in drinking water should be less than 0.1 g.L⁻¹ [7]. Diazinon, which is an organophosphorus (PO), is employed to control different kinds of insects [8, 9]. It is classified by the World Health Organization (WHO) as “moderately hazardous” Class II. Low concentrations of diazinon (even 350 ng.L⁻¹) can be highly toxic to aquatic organisms. It has been found that fatal human doses are in the range of between 90 and 444 mgkg⁻¹. It is, thus, essential to use effective chemical and biological methods for treatment of wastewaters containing pesticides, particularly diazinon. Since most conventional ways cannot be applied to remove compounds like organic products existing in wastewaters from chemical, agrochemical and textile industries, application of advanced oxidation processes

(AOPs), in which high reactive HO radicals in driving oxidation processes capable of mineralizing even less reactive contaminants are created, is entirely vital [10–12]. Cheapness, complete degradation, decomposition of pollutants even at very low amounts and degradation of toxic materials without pollution transfer to another phase are a few benefits of AOPs [13–15]. WO_3 is defined as a material with good photochromic, electrochromic, gasochromic, and photocatalytic properties [16–18]. Further, compared to TiO_2 and ZnO , WO_3 is capable of absorbing more solar light in the visible region because its band gap is about 2.7 eV [16, 17]. However, when WO_3 is used separately, its photocatalytic activity is weak because of its relatively low conduction-band level (0.5 V vs) [16, 17]. For improving the photocatalytic characteristic of WO_3 , Fe, Pt, Cu, and CuBi_2O_4 are employed for synthesis and modification of it [16, 17, 19, 20]. It should be pointed that the multielectron O_2 reduction can increase the photocatalytic activity of these materials. The magnetic separation, which is an environmentally benign method, has been used by many researchers as it creates no pollutants and can remove huge volumes of effluents in a very short time [21]. A magnetic composite, which is widely used, is Fe_3O_4 having superparamagnetic characteristics and can be recovered by means of an external magnetic field and reused without losing the active sites. Thus, because of the high conductivity of Fe_3O_4 and CB level (1 V vs. NHE), we were convinced to apply it in concert with WO_3 for improving photocatalytic efficiency through increasing charge transport. In recent years, many researchers have used the nanoparticles such as surface-modified Fe_3O_4 for treatment of effluents containing dyes even though the preparation of these magnetic adsorbents is not comfortable [22, 23]. Monolayers can be formed on several surfaces by aminosilane coupling agents; by doing this, the properties of the surface are changed and NH_2 groups are introduced into the modified surfaces. It has been reported that an aminosilane was employed to modify the surfaces of magnetite particles for lipase immobilization, wear properties improvement, and DNA purification. It should be noted that more studies are needed to survey the photocatalytic characteristics of aminosilane modified Fe_3O_4 and other nanoparticles for wastewaters containing pesticides. The aminopropyltriethoxysilane (APTES) polymers are used for gaining cationic amine groups on magnetic particle. The grafting reaction conditions of APTES are easier and simpler in comparison with most organosilane molecules.

In this research, in the presence of UV irradiation Fe_3O_4 - WO_3 -APTES nanoparticles were first synthesized as a new catalyst. The nanoparticles were then used for photocatalytic degradation of diazinon from synthetic and real water samples. Also, the effects of operating variables like solution pH, catalyst dosage, initial diazinon concentration, different purging gases, H_2O_2 concentration, and type of organic compounds on the removal efficiency of diazinon were studied in presence of UV irradiation. Furthermore, a kinetic study was performed and simulated with the zero, first, second and Langmuir–Hinshelwood kinetic models. In order to investigate the cost-efficiency of the processes, the electrical energy per order (E_{EO}) was calculated.

2 Materials and methods

2.1 Chemicals

All chemicals: tungsten chloride, $\text{FeCl}_3 \cdot 6\text{H}_2\text{O}$, $\text{FeCl}_2 \cdot 4\text{H}_2\text{O}$, 3-aminopropyltriethoxysilane (APTES), sodium hydroxide, folic acid, citric acid, humic acid, oxalic acid, phenol, EDTA and hydrochloric acid were of the highest available quality and procured from Merck (Darmstadt, Germany) and used without further purification. Diazinon (O,O-diethyl O-[6-methyl-2-(1-methylethyl)-4-pyrimidinyl]) was obtained from Chem-service (USA). Table 1 presents the chemical structure and properties of diazinon. Figure 1 shows the absorption spectra of diazinon. The light source was supplied with a 125-W medium-pressure UVC lamp emitting a maximum wavelength at 247.3 nm. The light intensity of the UVC lamp was $1,020 \mu\text{Wcm}^{-2}$ recorded by a digital radiometer (Model DRC-100X, SPECTROLINE) combined with a DIX-365 radiation sensor (ShokofanTosee, Iran). The photocatalytic reactor utilized in a previous study was applied to remove diazinon [24]. The pH values were measured by a Metrohm model 713 pH-meter and NaOH or HCl (0.1 molL^{-1}) were used for adjusting pH.

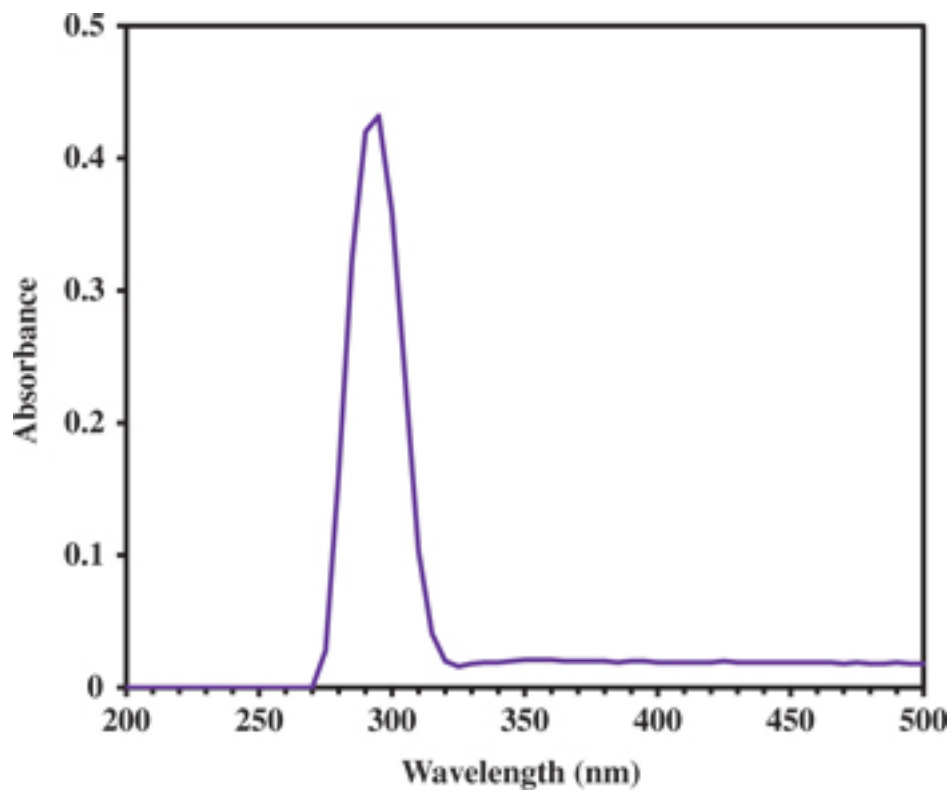
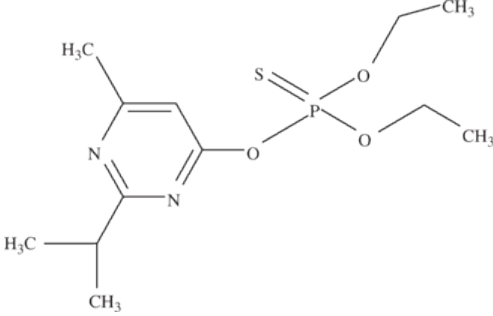


Figure 1: Absorption spectra of the diazinon.

Table 1: Chemical structure and characteristics of diazinon.

Structure	
	
Density (gmL ⁻¹ at 20 °C)	1.11
λ _{max} (nm)	300
M _w (gmol ⁻¹)	304.3
Solubility in water	40 mg/L
Vapor pressure	1.40 × 10 ⁻⁴ , 8.4 × 10 ⁻⁵ mmHg at 20 °C
Henry's constant	1.4 × 10 ⁻⁶ atm.m ³ mol ⁻¹
K _{ow}	2.5 × 10 ⁴
K _{oc}	40–854 Lkg ⁻¹ _{oc}

2.2 Synthesis of Fe₃O₄-WO₃- APTES nanoparticles

The Fe₃O₄-WO₃-APTES nanoparticles were synthesized by means of two simultaneous methods: co-precipitation and hydrothermal [21, 25, 26]. A schematic diagram of the preparation of the Fe₃O₄-WO₃- APTES nanoparticles has been shown in Figure 2. X-ray diffraction (XRD, Siemens D-5000, Germany), Fourier transform infrared spectroscopy (FT-IR), scanning electron microscopy (SEM, Mira3, Tescan, Czech Republic), energy dispersive X-ray (EDX), vibrating sample magnetometer (VSM, MDKFD, Iran), pH_{pzc} techniques were used for characterization of the prepared nanoparticles.

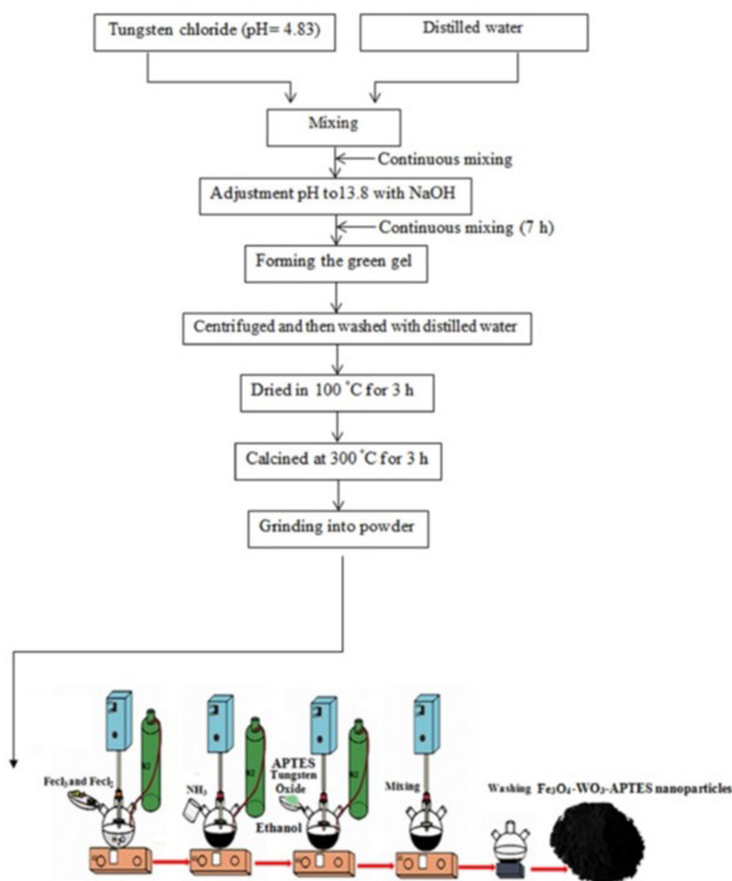


Figure 2: Schematic diagram of the preparation of the $\text{Fe}_3\text{O}_4\text{-WO}_3\text{-APTES}$ nanoparticles.

2.3 Experimental procedure and analysis

The fresh stock solutions of the pesticide containing $1,000 \text{ mg.L}^{-1}$ of diazinon were prepared weekly and stored at 4°C and the working samples were prepared daily by dilution of the stock solutions in doubled distilled water. A certain dose of the photocatalyst ($0.1\text{--}1 \text{ g.L}^{-1}$) was added to 1 L of the diazinon solution ($10\text{--}50 \text{ mg.L}^{-1}$) and, within all runs, the pH values were set from 3 to 11. All experiments were performed under ambient conditions for 2 h. The batch experiments were conducted at $25\pm 1^\circ\text{C}$ and continuously stirred. For the photocatalyst removal of the pesticide, a solution, containing known contents of diazinon and the nanocatalyst, was prepared and allowed to equilibrate for 30 min. A 125- W medium-pressure UVC lamp, placed into the batch photoreactor, was used for irradiation. At each stage, 10 mL of the suspension was taken at definite time intervals. The nanocatalyst was separated from the mixture solution by permanent magnet for 2 min. The residual contents of diazinon in all samples were detected via a spectrophotometer (UV /Vis Spectrophotometer, Hach-DR 5000, USA) at $\lambda_{\text{max}} = 300 \text{ nm}$ by a calibration curve depicted based on the Beer-Lambert law [27]. It should be noted that a few experiments were performed in triplicate and mean values of the data were reported. The error bars have not been shown in the figures because all standard deviations never exceeded $\pm 1.5\%$.

3 Results and discussion

3.1 Characterization of nanocatalyst

3.1.1 XRD analysis

The XRD patterns of the nanoparticles: WO_3 , Fe_3O_4 , $\text{Fe}_3\text{O}_4\text{-WO}_3$ and $\text{Fe}_3\text{O}_4\text{-WO}_3\text{-APTES}$ have been illustrated in Figure 3. The patterns exhibit the crystalline structure of both WO_3 and Fe_3O_4 even after coating the Fe_3O_4

nanoparticles onto WO_3 . The main peaks at 2θ values of 18.27, 21.16, 30.11, 30.21, 35.42, 35.53, 37.03, 37.18, 43.12 and 57.09 corresponded to the (011), (002), (112), (200), (121), (103), (022), (202), (004) and (321) planes of orthorhombic Fe_3O_4 (JCPDS card no. 031156) [25]. And, the main peaks at 2θ values of 23.707, 24.099, 26.587, 28.776, 34.022, 35.525, 41.524, 50.494, 54.302, 55.116, 57.677 and 62.446 corresponded to the (020), (200), (120), (111), (220), (121), (221), (112), (041), (401), (331) and (430) planes of orthorhombic crystalline WO_3 (JCPDS card no. 36-1451) [13]. As illustrated in Figure 3, the XRD peaks related to the nanoparticles of Fe_3O_4 and WO_3 are still observed after the modification with APTES. These results indicate the formation of mixture of Fe_3O_4 and WO_3 nanoparticles and APTES. The average crystalline size of the WO_3 , Fe_3O_4 , $\text{Fe}_3\text{O}_4\text{-WO}_3$ and $\text{Fe}_3\text{O}_4\text{-WO}_3\text{-APTES}$ nanoparticles were calculated with the Debye–Scherrer's equation. The mean crystallite size of the nanoparticles: WO_3 , Fe_3O_4 , $\text{Fe}_3\text{O}_4\text{-WO}_3$ and $\text{Fe}_3\text{O}_4\text{-WO}_3\text{-APTES}$ were estimated to be 23, 8, 19 and 19.3 nm, respectively.

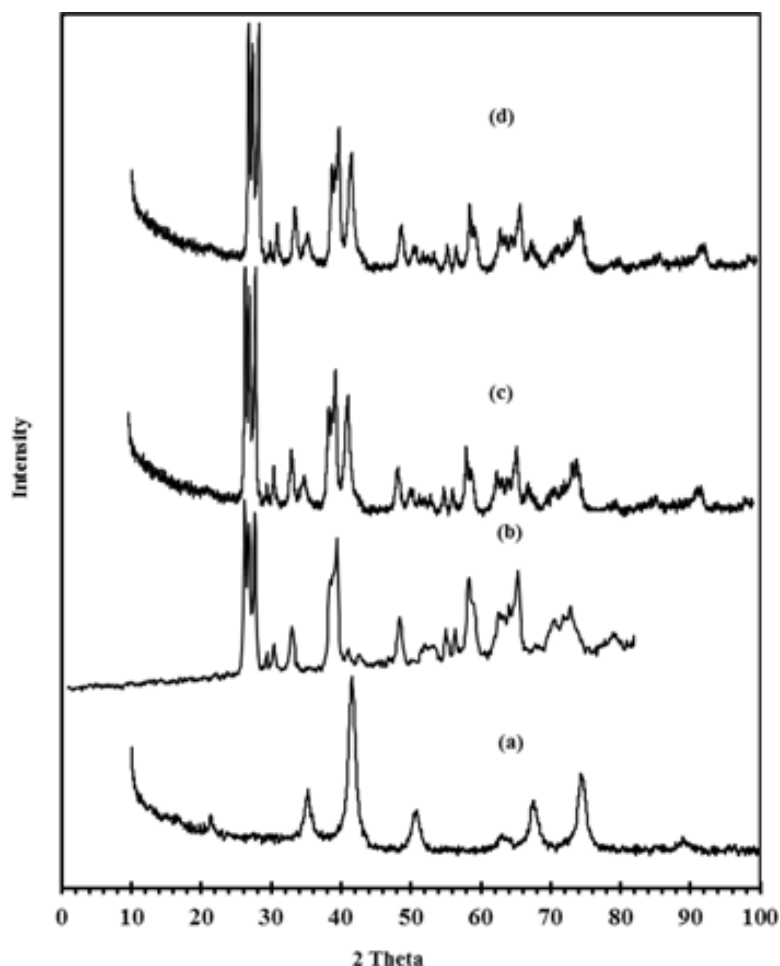


Figure 3: XRD image of the samples: (a) Fe_3O_4 (b) WO_3 (c) $\text{Fe}_3\text{O}_4\text{-WO}_3$ (d) $\text{Fe}_3\text{O}_4\text{-WO}_3\text{-APTES}$.

3.1.2 FT-IR analysis

Since photocatalytic reactions often take place on nanocatalysts' surface, the functional groups on the surface of the nanocatalysts are very important. Thus, the FT-IR analysis on the surface of the nanoparticles: WO_3 , Fe_3O_4 , $\text{Fe}_3\text{O}_4\text{-WO}_3$ and $\text{Fe}_3\text{O}_4\text{-WO}_3\text{-APTES}$ nanoparticles was performed in the range of $400\text{--}4,000\text{ cm}^{-1}$ (Figure 4). The Fe_3O_4 nanoparticles showed significant absorption peaks at 447, 580, 860, 1,403, 1,623, 3,378, 3,788, and $3,850\text{ cm}^{-1}$ [25]. Also, the FT-IR spectrum of the WO_3 nanoparticles showed significant absorption peaks at 817.40, 1,449.94, 1,639.29, 2,360.37 and $3,398.37\text{ cm}^{-1}$ [13]. The FT-IR spectrum of the $\text{Fe}_3\text{O}_4\text{-WO}_3$ nanoparticles presented significant absorption peaks at 445.85, 573.99, 813.4, 940.17, 1,395.19, 1,624.45, 2,360.99 and $3,385.3\text{ cm}^{-1}$. FT-IR spectrum of the $\text{Fe}_3\text{O}_4\text{-WO}_3\text{-APTES}$ nanoparticles indicated significant absorption peaks at 444.19, 577.47, 793.93, 944.77, 1,114.47, 1,221.31, 1,385.18, 1,507.55, 1,629.27, 2,361.09, 3,410.10, 3,741.3 and $3,853.91\text{ cm}^{-1}$. The two distinct absorption peaks at 580 and 447 cm^{-1} are attributed to the vibrations of $\text{Fe}^{3+}\text{-O}^{2-}$ and $\text{Fe}^{2+}\text{-O}^{2-}$, respectively [25]. The peaks between 700 and 900 cm^{-1} are assigned to the aromatic C-H stretching. The peak at $3,400\text{ cm}^{-1}$ belongs to vibration of -OH group. For the Fe_3O_4 nanoparticles, the band observed between 600 and 800 cm^{-1} corresponds to $\nu(\text{W-O}_{\text{inter}}\text{-W})$ and $\nu(\text{W-O}_{\text{intra}}\text{-W})$ [13]. For the WO_3 nanoparticles,

the band observed between 2,800 and 3,500 cm^{-1} corresponds to the $\nu(\text{HOH})$ and $\nu(\text{OH})$ [13]. The band observed between 1,600 and 1,650 cm^{-1} corresponds to $\delta \text{H}_2\text{O}$ [13]. The FT-IR analysis supported coating the Fe_3O_4 nanoparticles onto the WO_3 nanoparticles. After amine-modified Fe_3O_4 - WO_3 nanoparticles with APTES, the new peaks at 1,507.55, 1,385.18, 557.47 and 600–800 cm^{-1} corresponding to N–H, C–N bending vibration, Fe–O vibration of Fe_3O_4 and $\nu(\text{W-O}_{\text{inter}}\text{-W})$ and $\nu(\text{W-O}_{\text{intra}}\text{-W})$ were seen in the spectrum of the Fe_3O_4 - WO_3 -APTES nanoparticles. These observations evidence that amine groups have been successfully introduced on the surface of the Fe_3O_4 - WO_3 nanoparticles, forming the APTES - Fe_3O_4 - WO_3 nanocatalyst.

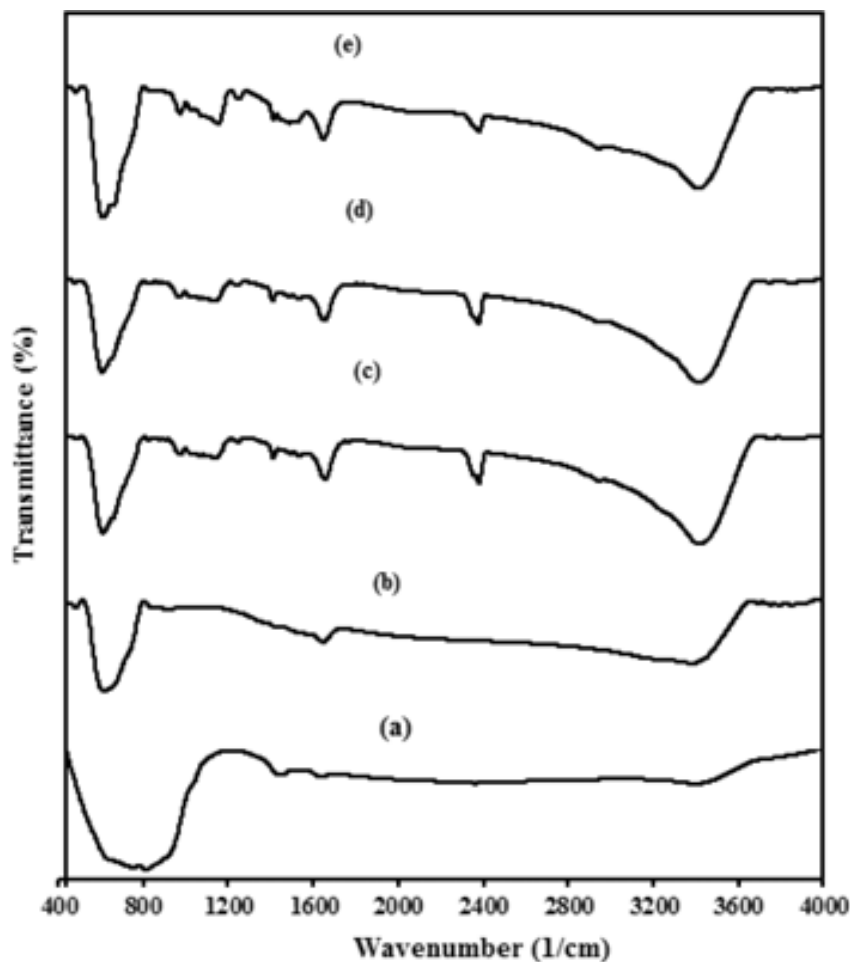


Figure 4: FT-IR image of the samples: (a) Fe_3O_4 (b) WO_3 (c) Fe_3O_4 - WO_3 (d) Fe_3O_4 - WO_3 -APTES (E) Recovery.

3.1.3 SEM, EDX and VSM analysis

Scanning electronic microscopy (SEM) was used to investigate the morphology, shape and size of the WO_3 , Fe_3O_4 , Fe_3O_4 - WO_3 and Fe_3O_4 - WO_3 -APTES nanoparticles. The SEM images of the WO_3 , Fe_3O_4 , Fe_3O_4 - WO_3 and Fe_3O_4 - WO_3 -APTES nanoparticles have been shown in Figure 5-Figure 5, respectively. Figure 5 clearly illustrates the distribution of APTES on the surface of the Fe_3O_4 - WO_3 nanoparticles. Also, Figure 5 shows the sphere structure for the Fe_3O_4 - WO_3 -APTES nanoparticles. The EDX patterns of the Fe_3O_4 , Fe_3O_4 - WO_3 and Fe_3O_4 - WO_3 -APTES nanoparticles have been presented in Figure 6. According to the results of EDX analysis, weight percentages of C, O and Fe in Fe_3O_4 nanoparticles were 20.94, 26.07 and 45.28 %, weight percentages of O, Fe and W in Fe_3O_4 - WO_3 nanoparticles were 12.53, 78.29 and 11.68 %, and weight percentages of C, O, Fe and W in Fe_3O_4 - WO_3 -APTES nanoparticles were 2.06, 21.19, 64.29 and 9.98 %, respectively. Therefore, the synthesized compound was composed of Fe, O, and W, indicating the formation of the Fe_3O_4 - WO_3 -APTES nanoparticles. VSM magnetization curve of the samples at room temperature has been depicted in Figure 6. The saturated magnetization values were 58.97, 43.83, 42.74 and 0.0043 emu g^{-1} , respectively, for the Fe_3O_4 , Fe_3O_4 - WO_3 -APTES, Fe_3O_4 - WO_3 and WO_3 nanoparticles.

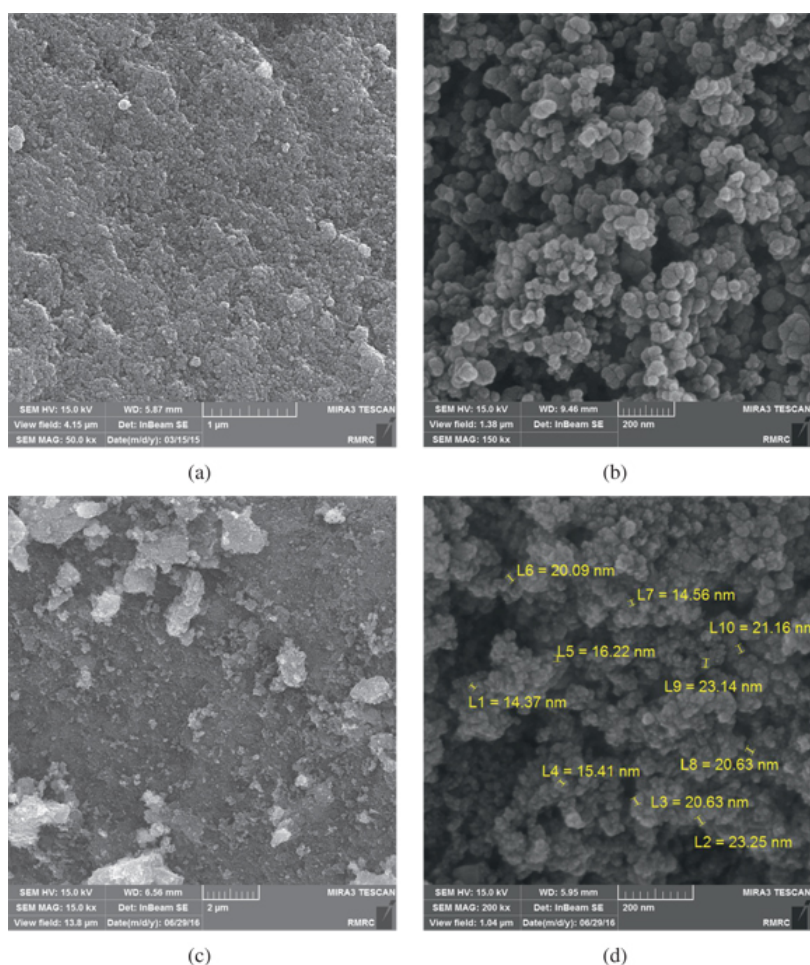


Figure 5: SEM images of the samples: (a) Fe₃O₄ (b) WO₃ (c) Fe₃O₄-WO₃ (d) Fe₃O₄-WO₃-APTES.

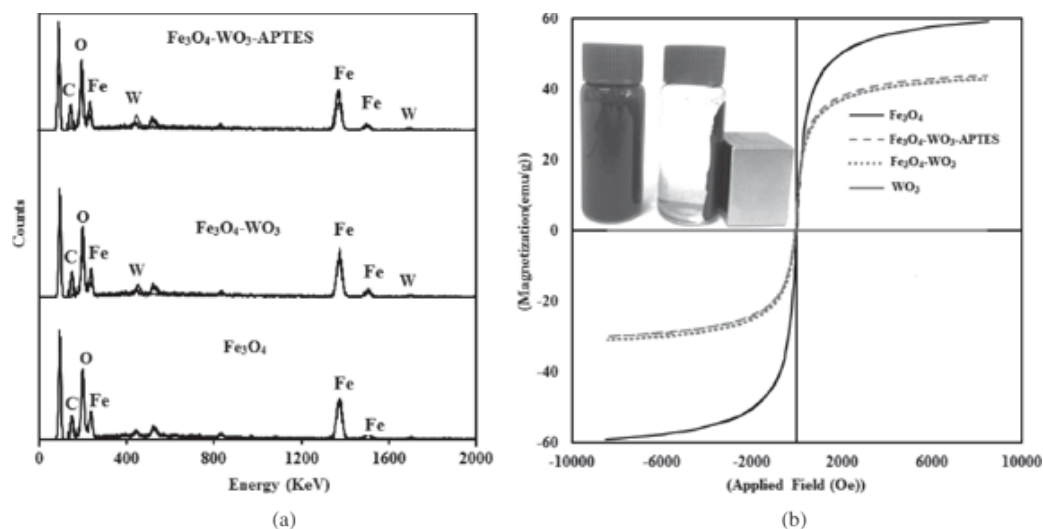


Figure 6: (a) EDX image of the samples, (b) VSM image of the samples.

3.2 Effects of operational parameters on the photocatalytic degradation of diazinon

3.2.1 Effect of initial pH

In this study, pH levels were set between 3 and 11 for studying the pH impact on diazinon removal at the constant dose of 0.25 g.L⁻¹ of the Fe₃O₄-WO₃-APTES nanoparticles. It should be noted that the pH value was 5.63 at the beginning of the reaction. Generally, the degradation efficiency fluctuated widely by changing the

levels of pH; at pH values of 3, 5, 6, 7, 8, 9 and 11, respectively, 58.42, 88.9, 91.4, 96.4, 75.15, 45.15 and 33.88 % of diazinon was removed (Figure 7). As can clearly be seen, the highest removal efficiency happened at pH 7 because, in either acidic or basic conditions, the APTES nanoparticles are corroded. The values of pH_{pzc} of the WO_3 , Fe_3O_4 , $Fe_3O_4-WO_3$ and $Fe_3O_4-WO_3-APTES$ nanoparticles were 5.09, 6, 7.03 and 8.22, respectively. It can be pointed that at different pH levels various electrostatic reactions take place between on the surface of the $Fe_3O_4-WO_3-APTES$ nanoparticles and the pesticide [8, 28]. The value of pK_a of diazinon was found to be 2.6 [14], in which the nanoparticles of $Fe_3O_4-WO_3-APTES$ are positively charged and negatively charged at pH values of below 8.2 and above 2.6, respectively. The positively charged $Fe_3O_4-WO_3-APTES$ nanoparticles and negatively charged diazinon molecules can quickly attract together in an optimal condition in which pH ranges from $pK_a^{diazinon}$ to $pH_{pzc}^{Fe_3O_4-WO_3-APTES}$. A lower extent of adsorption was observed on the nanoparticles' surface, at high pHs, as both diazinon and the $Fe_3O_4-WO_3-APTES$ nanoparticles are negatively charged and, in turn, the electrostatic repulsion happens between them [8, 28]. As mentioned above, the highest performance was seen at the pH value of 7; therefore, all other experiments were carried out at this level.

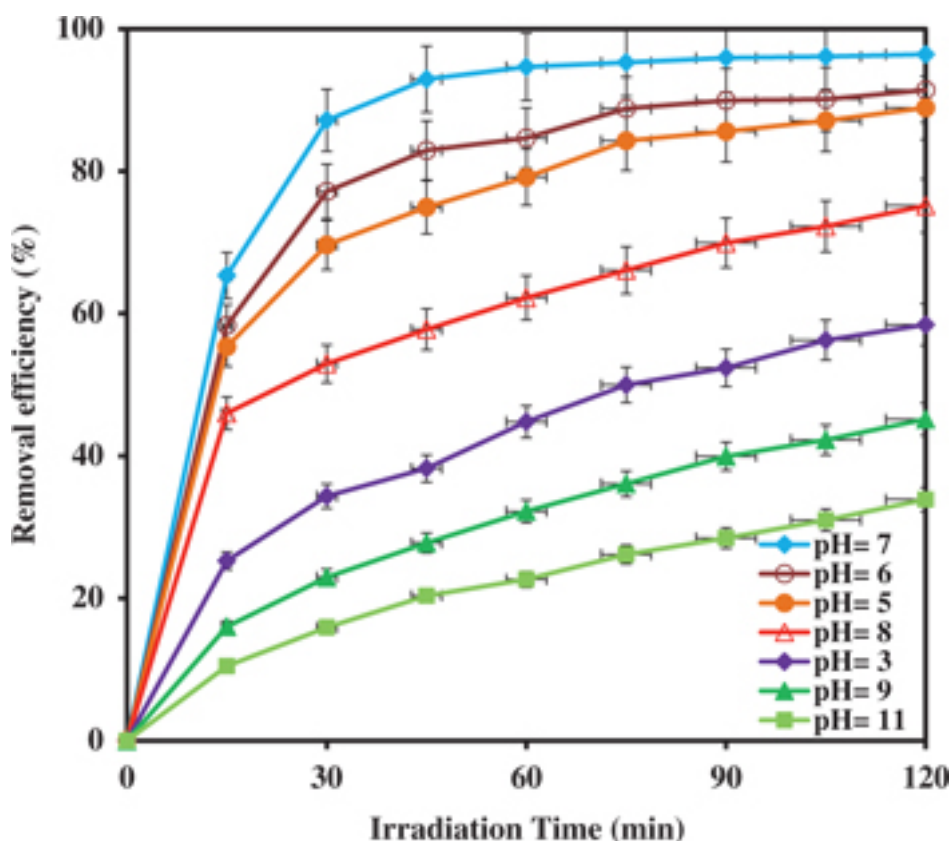


Figure 7: Effect of initial pH on the photocatalytic removal of diazinon (catalyst dosage= 0.25 g.L^{-1} , $[\text{diazinon}]_0 = 20 \text{ mg.L}^{-1}$).

3.2.2 Effect of photocatalyst dosage

In the present research, different doses ($0.1\text{--}1 \text{ g.L}^{-1}$) of the nanocatalyst were used to evaluate the removal efficiency of the pesticide at the constant amount of diazinon (20 mg.L^{-1}) and pH of 7. As can be seen in Figure 8, a marginal efficiency was observed at time zero (without UV irradiation) for different dosages. The removal efficiency improved between 68.7 and 96.4 % with raising the dose of the nanocatalyst between 0.1 to 0.25 g.L^{-1} . After that, a downward trend was seen in efficiency. The main reasons for this improvement in removal efficiency are as follows: when the dose of the nanocatalyst is raised, there will be more diazinon molecules that can be adsorbed on the surface of the catalyst and the density of catalyst particles increases in the area of illumination [8, 9, 28, 29]. In the case of catalyst doses higher than 0.25 g.L^{-1} , a downward trend was experienced in diazinon removal as light scattering decreasing the aggregation and the activity of the catalyst particles takes place. In this study, the dose of 0.25 g.L^{-1} was selected as the optimal value for the $Fe_3O_4-WO_3-APTES$ nanoparticles. The highest removal efficiency happened at the photocatalyst dose of 0.25 g.L^{-1} . Therefore, more examinations were performed at this value. It should be stated that the photocatalytic reduction of diazinon went up between 65.32 and 96.4 % with rising time of irradiation from 15 to 120 min.

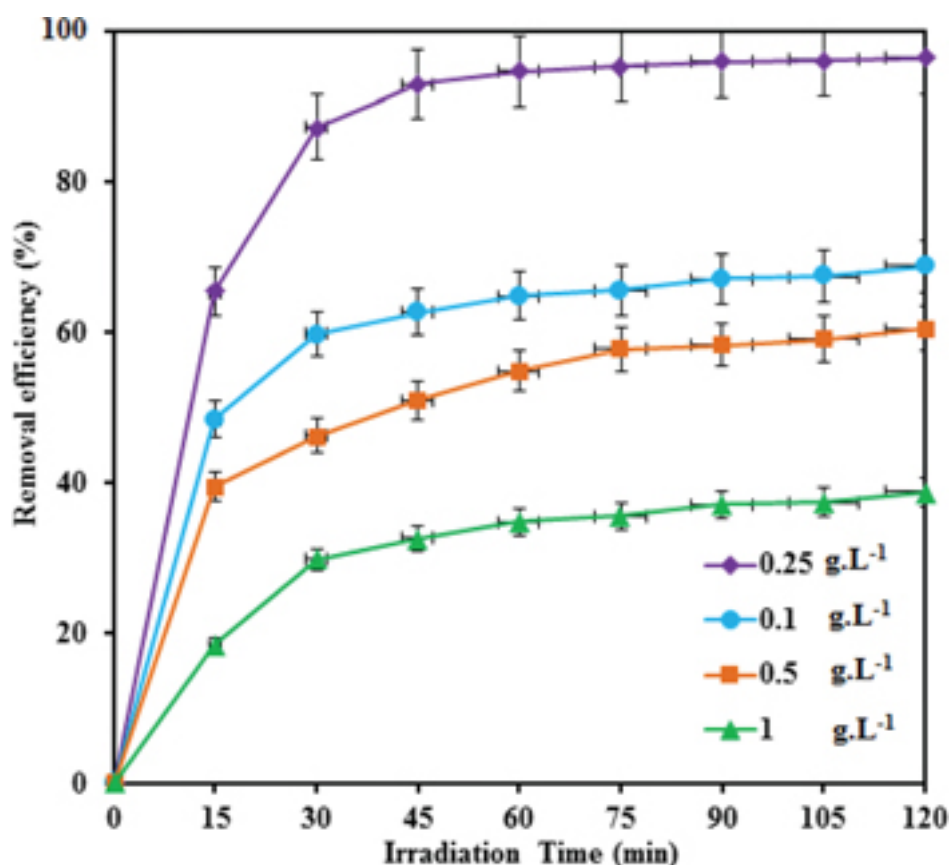


Figure 8: Effect of catalyst dosage on the photocatalytic removal of diazinon (pH= 7, [diazinon]₀= 20 mg.L⁻¹).

3.2.3 Kinetics and electrical energy studies

For investigation of the kinetic information, some examinations were done under the following conditions: initial diazinon concentration of 10, 20, 30, 40, 50 mg.L⁻¹, initial pH of 7 and constant nanocatalyst dose of 0.25 g.L⁻¹. In order to achieve the kinetic information, the zero, first and second order equations (eqs (1)–(3)) were used [8, 30]:

$$[\text{diazinon}]_0 - [\text{diazinon}]_t = k_0 t \quad (1)$$

$$\ln \frac{[\text{diazinon}]_0}{[\text{diazinon}]_t} = k_{\text{obs}} t \quad (2)$$

$$\frac{1}{[\text{diazinon}]_t} - \frac{1}{[\text{diazinon}]_0} = k_2 t \quad (3)$$

where [Diazinon]₀ is the initial concentration of diazinon (mg.L⁻¹), k_0 (mol.L⁻¹ min⁻¹), k_{obs} (min⁻¹) and k_2 (L mol⁻¹ min⁻¹). So as to attain kinetic variables for the photocatalytic destruction of the pesticide, $C_0 - C_t$, $\ln[C_0/C_t]$ and $\frac{1}{C_t} - \frac{1}{C_0}$ versus t was plotted. The k_{obs} values at different initial concentrations (Table 2) were calculated from the slope between $\ln([\text{Diazinon}]_0/[\text{Diazinon}])$ versus reaction time. Table 2 presents a breakdown of the kinetic variables of zero, first and second-order reactions for the removal efficiency at different initial diazinon concentrations. The first-order model explained better the photocatalytic degradation rate.

Table 2: Kinetic parameters for the photocatalytic degradation of diazinon at different initial concentrations of diazinon (Fe₃O₄-WO₃-APTES dosage= 0.25 g.L⁻¹, and pH =7).

[Diazinon] ₀ (mg L ⁻¹)	Zero-order		First-order			Second-order	
	k_0	R ²	k_{obs}	(k_{obs}) ⁻¹	R ²	E_{Eo} (kWhm ⁻³)	k_2 R ²

	(mol L ⁻¹ min ⁻¹)		(min ⁻¹)	(min)			(L mol ⁻¹ min ⁻¹)	
10	0.1787	0.8802	0.1008	9.92	0.9729	47.62	0.0337	0.9189
20	0.2172	0.6684	0.0497	20.12	0.9519	96.58	0.012	0.9635
30	0.1601	0.7803	0.0118	84.74	0.941	406.78	0.001	0.9886
40	0.1787	0.8802	0.0069	144.92	0.9403	695.65	0.0003	0.9793
50	0.1899	0.8983	0.0051	196.074	0.9297	941.18	0.0001	0.9537

As can be seen from eqs (4) and (5), the relationship between the first-order rate constant (k_{obs}) and initial diazinon concentration was described better by the Langmuir–Hinshelwood (L-H) model [8, 30].

$$-\frac{d[\text{Diazinon}]}{dt} = \frac{k_c K_{\text{Diazinon}} [\text{Diazinon}]}{1 + K_{\text{Diazinon}} [\text{Diazinon}]_0} = k_{\text{obs}} [\text{Diazinon}] \quad (4)$$

$$\frac{1}{k_{\text{obs}}} = \frac{1}{k_c K_{\text{Diazinon}}} + \frac{[\text{Diazinon}]_0}{k_c} \quad (5)$$

where k_c (mg.L⁻¹ min⁻¹) is the kinetic rate constant of surface reaction and K_{Diazinon} (mg.L⁻¹)⁻¹ is the Langmuir adsorption constant. K_{Diazinon} and k_c were 0.085 (Lmg⁻¹) and 0.2016 (mg.L⁻¹ min⁻¹) by plotting (k_{obs})⁻¹ versus initial concentration of diazinon, respectively.

E_{EO} value, which is the number of kWh of electrical energy required to decline the content of a contaminant by 1 order of magnitude (90 %) in 1 m³ of polluted water, of the photocatalytic reduction of the pesticide was studied in terms of economic views (eq. (6) and (7)).

$$E_{\text{EO}} = \frac{38.4 \times P}{V \times k_{\text{obs}}} \quad (6)$$

$$E_{\text{EO}} = \frac{p \times t \times 1000}{V \times 60 \times \log ([\text{diazinon}]_i / [\text{diazinon}]_f)} \quad (7)$$

where P is the sum of input power (kW), t is the irradiation time (min), V is the volume (L) of the wastewater, and k_{obs} is the first-order rate constant (min⁻¹) for the decay of the pollutant. The E_{EO} values for the processes studied in this research have been shown in Table 2. As can be seen, the E_{EO} value raised between 47.62 and 941.18 kWhm⁻³ by rising diazinon content between 10 and 50 mg.L⁻¹. Furthermore, the process of UV/Fe₃O₄-WO₃-APTES had the lowest E_{EO} value (172.44 kWhm⁻³) as compared with other methods: UV/WO₃ (672.74 kWhm⁻³), UV/Fe₃O₄ (845.02 kWhm⁻³), UV (1,016.11 kWhm⁻³) and UV/Fe₃O₄-WO₃ (18,898.92 kWhm⁻³).

3.2.4 Effect of different purging gases

In order to study the impact of the variable of purging gases, oxygen and nitrogen gases at 2 L.min⁻¹ flow rate were used under the condition: Fe₃O₄-WO₃-APTES nanoparticle dosage of 0.25 g.L⁻¹, constant diazinon concentration of 20 mg.L⁻¹ and pH of 7. The impacts of purging gases and change of DO content have been presented in Figure 9. As can be clearly seen, in the presence of both gases, the process experienced a lower efficiency compared the method in which no gas was utilized. In ambient condition, the removal efficiency boosted by 31.08 % when time was raised from 15 to 120 min. And, in the case of oxygen and nitrogen, the efficiencies ranged between 53.44 to 83.83 % and 27.29 to 61.68 %, respectively. Since O₂ and N₂ gases serve as an electron scavenger competing with diazinon ions for capturing electrons, using these gases results in a decrease in efficiency [8].

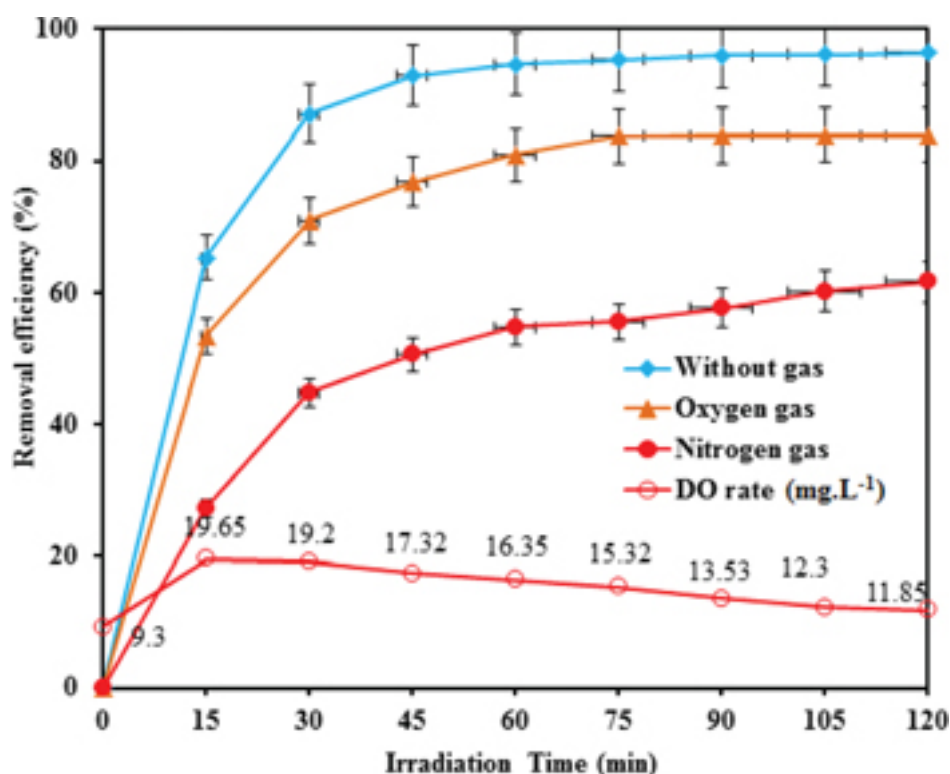


Figure 9: Effect of different purging gases and variation of DO concentration during the photocatalytic removal of diazinon (catalyst dosage = 0.25 g.L^{-1} , pH = 7, $[\text{diazinon}]_0 = 20 \text{ mg.L}^{-1}$).

3.2.5 Effect of hydrogen peroxide

It is imperative that the optimum value of H_2O_2 be selected because it raises the photocatalytic performance. It should be pointed that the type and quantity of contaminants influence the selection of this optimum point. In this study, the effect of different H_2O_2 concentrations (2–50 mM) on the removal efficiency was investigated under the conditions: diazinon concentration of 20 mg.L^{-1} , $\text{Fe}_3\text{O}_4\text{-WO}_3\text{-APTES}$ nanoparticle dosage of 0.25 g.L^{-1} , and pH of 7. It can be seen in Figure 10 that a rise in the content of H_2O_2 , the efficiency went up between 96.4 and 99.23 %, but it dropped to 47.23 % at the concentration of 50 mM. H_2O_2 can react with electron in the conduction band of $\text{Fe}_3\text{O}_4\text{-WO}_3\text{-APTES}$ nanoparticles, leading to an enhancement in diazinon removal. Equations (8) and (9) state that H_2O_2 can prevent the electron–hole recombination [31, 32]. H_2O_2 can act as an alternative electron acceptor to oxygen because it is a better electron acceptor than dissolved oxygen. Hence, a significant improvement in diazinon removal is expected in the case of low contents of H_2O_2 on account of the inhibition of the electron–hole recombination. Since H_2O_2 is a powerful scavenger of electron and $\bullet\text{OH}$, at high concentrations of H_2O_2 , the reaction between diazinon and positive holes or $\bullet\text{OH}$ in the valence band of the $\text{Fe}_3\text{O}_4\text{-WO}_3\text{-APTES}$ nanoparticles can be inhibited.



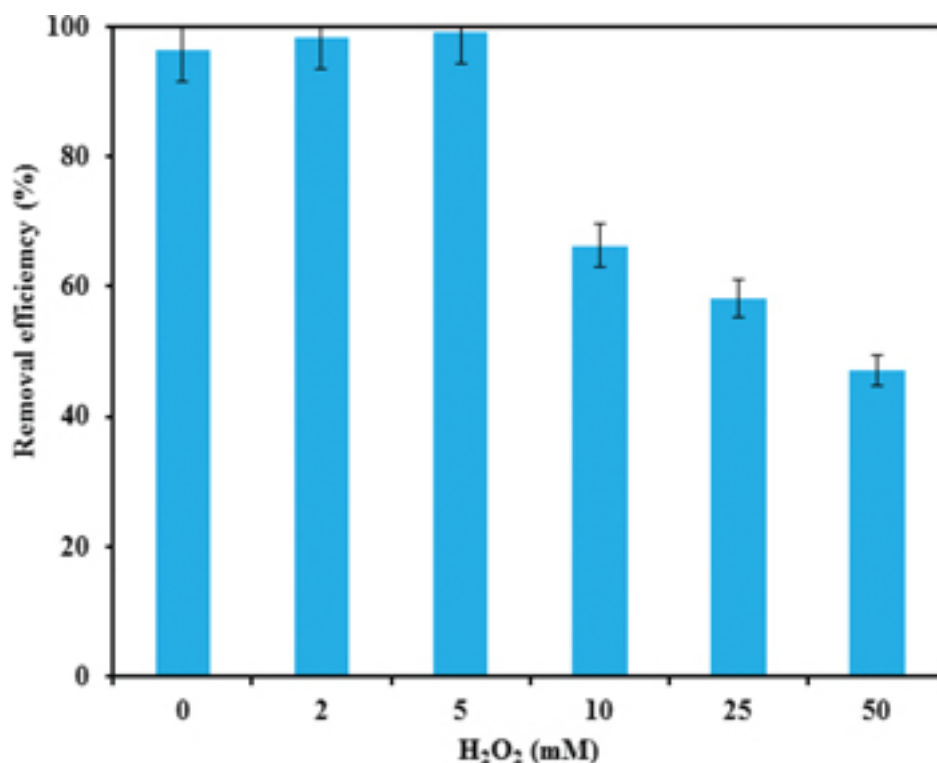


Figure 10: Effect of hydrogen peroxide on the photocatalytic removal of diazinon (catalyst dosage = 0.25 g.L^{-1} , pH= 7, $[\text{diazinon}]_0 = 20 \text{ mg.L}^{-1}$).

3.2.6 Effect of organic compounds

A few organic combinations: citric acid, folic acid, EDTA, oxalic acid, phenol and humic acid (equal to 20 mg.L^{-1}) were used in the present study to investigate the influence of these matters on the efficiency under the following conditions: initial diazinon content of 20 mg.L^{-1} , $\text{Fe}_3\text{O}_4\text{-WO}_3\text{-APTES}$ nanoparticles dosage of 0.25 g.L^{-1} and initial pH of 7. Figure 11 illustrates that 96.4, 70.3, 69.32, 67.37, 65.23, 60.12 and 3.22 % of the pesticide was removed in the case of without organic compounds, citric acid, folic acid, EDTA, oxalic acid, phenol and humic acid, respectively. Addition of an organic compound results in a decrease in the efficiency because of the fact that the interference happens among adsorbed organic molecules; as a result, the diazinon molecules do not have access to photocatalyst's surface [8, 13]. The structure of organic compounds is comprised of many aliphatic and aromatic organic molecules that can occupy the photoactive sites on the surface of the nanocatalyst. Also, these molecules that are subject to the same chemistry as the target analyte can leave fewer sites capable of removing diazinon molecules. Therefore, a slow degradation of diazinon is expected to happen due to competition among molecules.

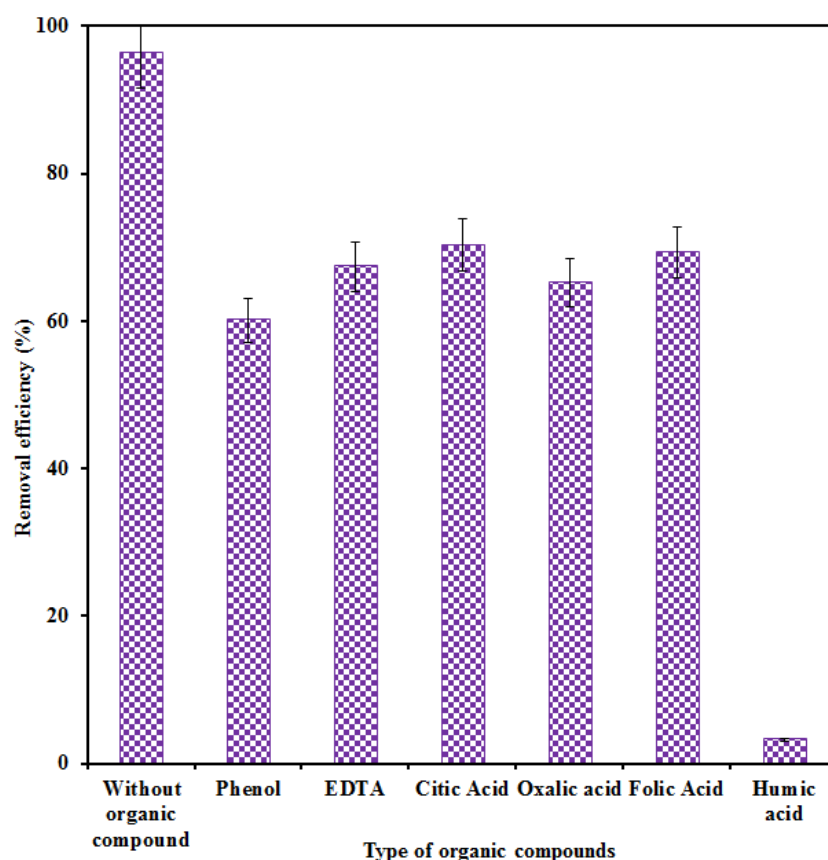


Figure 11: Effect of different organic compounds on the photocatalytic removal of diazinon (catalyst dosage= 0.25 g.L^{-1} , pH= 7, $[\text{diazinon}]_0=20 \text{ mg.L}^{-1}$, organic compounds= 20 mg.L^{-1}).

3.2.7 The comparison of each process and reusability

In this research, the performances of some photocatalytic methods: $\text{Fe}_3\text{O}_4\text{-WO}_3$ -alone, $\text{UV/Fe}_3\text{O}_4\text{-WO}_3$, $\text{Fe}_3\text{O}_4\text{-WO}_3\text{-APTES}$ -alone, WO_3 -alone, Fe_3O_4 -alone, UV-alone, $\text{UV/Fe}_3\text{O}_4$, UV/WO_3 and $\text{UV/Fe}_3\text{O}_4\text{-WO}_3\text{-APTES}$ were studied and compared at the same optimum reaction conditions at initial diazinon concentration of 20 mg.L^{-1} , nanoparticle dose of 0.25 g.L^{-1} and initial pH of 7. Removal efficiencies for the processes were 4.97, 2.97, 2.98, 17.97, 23.52, 43.27, 49.38, 57.48, and 96.4 % respectively (Figure 12). When adsorption was applied separately, it could not remove the pesticide dramatically. But the highest removal efficiency was achieved by the $\text{UV/Fe}_3\text{O}_4\text{-WO}_3\text{-APTES}$ method. The results of the photocatalytic reduction of diazinon via the $\text{UV/Fe}_3\text{O}_4\text{-WO}_3\text{-APTES}$ method extracted in this research were compared with other reported data. The efficiencies and kinetics parameters of the processes have been compared in Table 3. The findings indicated that the catalyst of $\text{UV/Fe}_3\text{O}_4\text{-WO}_3\text{-APTES}$ is suitable to remove this pesticide from aqueous media as compared with Fe_3O_4 and WO_3 -alone. In other words, the synergistic effect between Fe_3O_4 and WO_3 is entirely useful in the photocatalytic characteristics of $\text{UV/Fe}_3\text{O}_4\text{-WO}_3\text{-APTES}$. Since the CB level of Fe_3O_4 is lower, the photogenerated electrons are transferred from the surface of WO_3 to Fe_3O_4 [13, 21, 26]. Moreover, since the conductivity of Fe_3O_4 is by far higher than that of WO_3 , the transport rate of the electrons is quick, thereby declining the recombination of the photogenerated electrons and holes. Also, owing to the interface effects (like potential barrier) of the hybrid process of $\text{Fe}_3\text{O}_4/\text{WO}_3$, a decline in recombination of photogenerated electron-hole pairs is expected. The collected electrons may be used by a multielectron O_2 reduction mechanism.

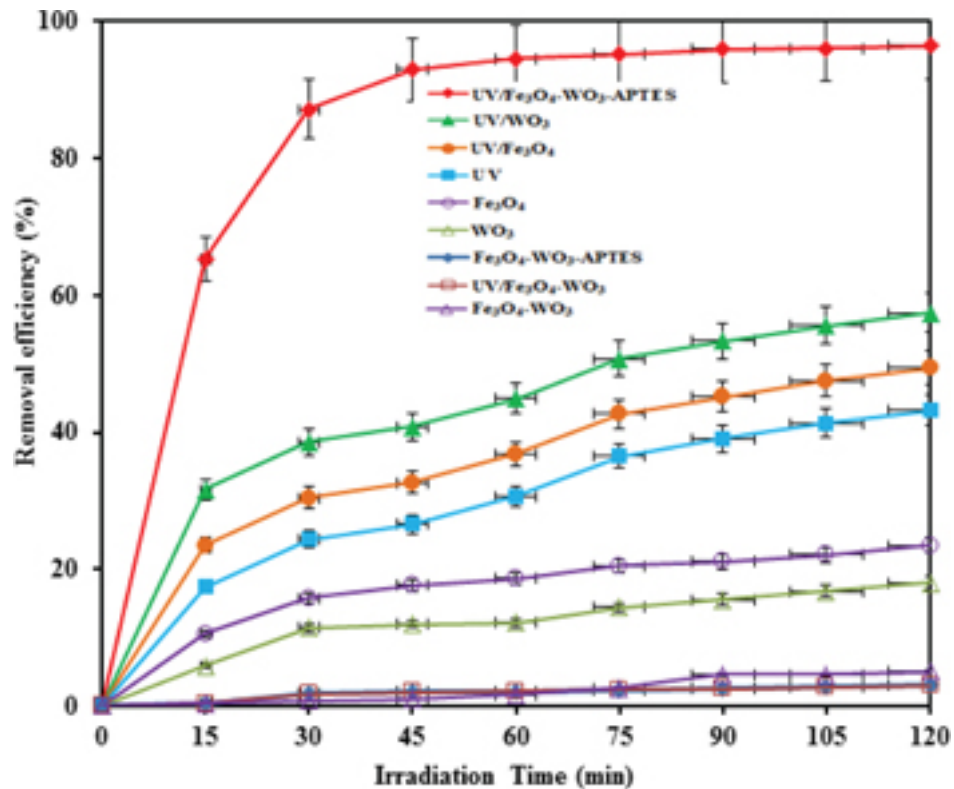


Figure 12: Contribution of each process involved in the photocatalytic removal of diazinon (catalyst dosage= 0.25 g.L⁻¹, pH= 7, [diazinon]₀=20 mg.L⁻¹).

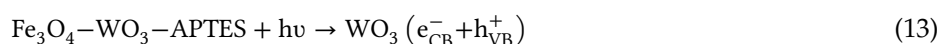
Table 3: Comparison of photocatalytic degradation of diazinon.

Systems	PH	Cat- alyst dosage (g.L ⁻¹)	[Diazinon] ₀ (mg.L ⁻¹)	Lamp (W)	Time (min)	Removal effi- ciency (%)	L-H parameters K _{diazinon} (Lmg ⁻¹)	k _c (mg L ⁻¹ min ⁻¹)	k _{obs} (min ⁻¹)	R ²	Ref- er- ence
Solar/N doped TiO ₂	7	2.5	10	350 Xenon	180	85	–	–	–	0.95	[29]
UV/WO ₃	7	0.5	20	125	120	99.88	0.068	0.006	0.057	0.9892	[13]
UV/ZnO- Scallop Shell	7	0.5	20	125	120	98.92	0.067	0.926	0.0343	0.987	[24]
UV/ZnO-TiO ₂	7	0.5	20	125	120	87.26	0.084	0.054	0.0158	0.978	[8]
UV/TiO ₂ - aeration	6	0.55	40	125	95	100	–	–	0.038	0.97	[39]
FeFNS-TiO ₂ /LED	7	0.1	1.3	3 mW	100	Degra- dation= 87.6	–	–	Degra- da- tion= 0.973 h ⁻¹	Degra- da- tion= 0.9922	[40]
						Mineral- ization= 67.9			Min- eral- iza- tion= 0.541 h ⁻¹	Min- eral- iza- tion= 0.9980	
UV/platinized TiO ₂	4.3	0.02	30	Xe 990	30	100	–	–	–	–	[14]
UV/ZnO	neu- tral	0.15	20	30	80	80	1.425	0.437	0.027	0.98	[30]
UV/TiO ₂	7	0.09	10	Xe 1500	180	100	–	–	0.0236	–	[41]
TiO ₂ /Visible light	nat- u- ral	Slurry TiO ₂ = 0.27	10	Xenon= 1,500 W	Re- moval= 60	Re- moval= 100	–	–	0.0714	–	[41]

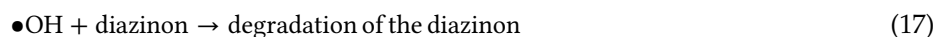
						Mineral- ization= 75					
Fe ₃ O ₄ -WO ₃ - APTES/UV	7	0.25	20	125	120	96.4	0.085	0.2016	0.0497	0.9519	This study

Based on the above experiments and analysis, a plausible mechanism for the photocatalysis can be proposed as follows:

When Fe₃O₄-WO₃-APTES is illuminated with the UV light ($\lambda < 390$ nm), an electron excites from the valence band to the conduction band to give separation of electron and hole (eq. 13):



Next, the electron can react with O₂ and H₂O₂. Further, positive hole reacts with H₂O or OH⁻ to create highly reactive radical species like hydroxyl radicals, which can oxidize unselectively organic compounds and their degradation intermediates. Additionally, the holes can oxidize directly many contaminants [13, 21, 26, 30].



Another reason for the mechanism of performance improvement degradation of diazinon is, the APTES behaves as Si-N co-doped in Fe₃O₄-WO₃ that can generate intermediate level between valence band and conduction band, thus not only reducing in the band gap but also restraining the electron-hole recombination. Further, the photocatalytic activity can be enhanced via the monolayer and/or multilayer of amino-silane, which can increase the oxygen chemisorption on the surface of Fe₃O₄-WO₃ [33].

Several researchers have stated the mechanism of diazinon decomposition; GC-MS tests have claimed that a few molecules and single ring structures are formed during the photocatalytic decomposition. Also, in many studies, the temporal distribution of species over the photocatalytic degradation of diazinon in aqueous environments via AOPs like ozonation and UV/H₂O₂ at different pH values has been surveyed [34, 35]. For instance, in the study by Shemer and Linden, 2-isopropyl-6-methyl-pyrimidin-4-ol and diethylthiophosphoric acid were found to be the products of the process: UV and UV/H₂O₂ [35]. And, Nakaoka *et al.* concluded that species such as 2-isopropyl-6-methyl-pyrimidin-4-ol, IMP and diazoxo are generated during the removal of this pesticide through Xe lamp/platinized TiO₂ [14]. Shirzad-Siboni *et al.* also applied the UV/Cu doped ZnO process for degradation of diazinon from aqueous environments and they reported that the following products are created: N-Benzyl-N-ethyl-p-isopropylbenzamide, Pentasiloxane, dodecamethyl-, Silane, cyclohexyldimethoxymethyl-, Tridecane, 1-iodo-, Hexadecane, Silane, (4-methoxyphenoxy)trimethyl-, Heptadecane, 8-methyl-, Decane, 2,4,6-trimethyl-, Tetradecane, 4-methyl-, Phenol, 2,4-bis(1,1-dimethylethyl)-, Dodecane, Tridecane, and 1-iodo [36].

Some authors have stated that sulfate ions are formed at a very early period of the diazinon degradation and then phosphate, carbonate and nitrate ions are generated. The structure of diazinon can express these results. The diazinon molecules detach sulfur groups, which are oxidized to sulfate ions. Many researchers have also reported similar findings and complete degradation pathways of organophosphorus pesticides in aqueous environments by AOPs [15, 30, 37, 38].

As the reusability of a photocatalyst is of great importance after reaction, the photocatalyst loaded with the pollutant was placed in the 2 M NaOH solution as a desorbing agent; all photocatalytic runs were repeated five times. It can be seen in Figure 13 that the UV/Fe₃O₄-WO₃-APTES showed quite similar photocatalytic activity after 120 min over five repeated experiments.

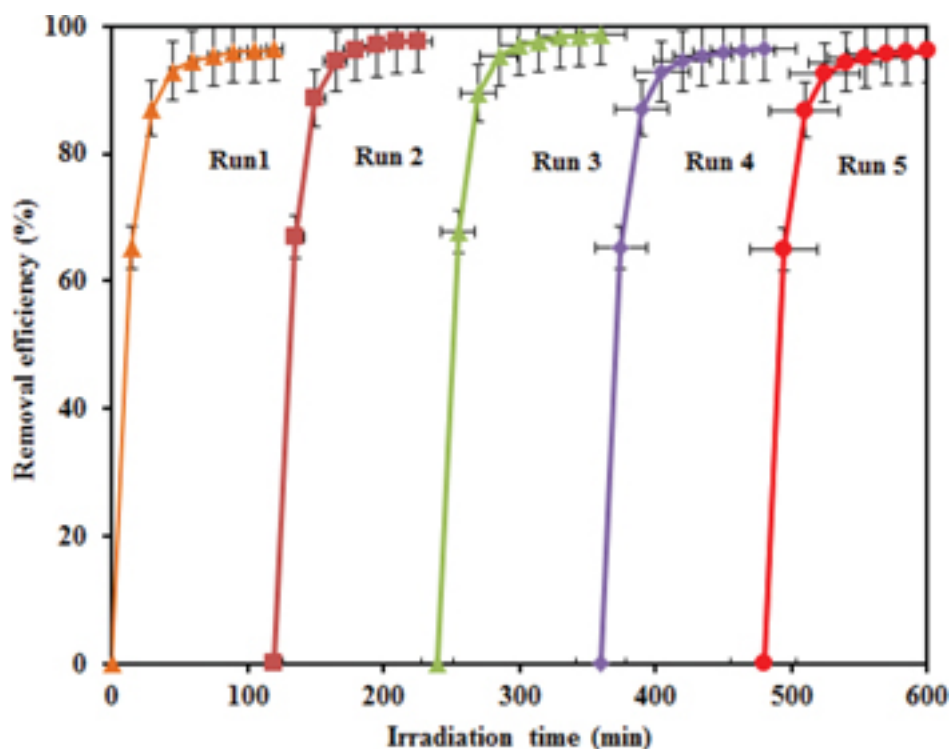


Figure 13: Reusability test for the photocatalytic removal of diazinon within five repeated cycles (catalyst dosage = 0.25 g.L^{-1} , $\text{pH} = 7$, $[\text{diazinon}]_0 = 20 \text{ mg.L}^{-1}$).

3.3 Removal of diazinon from real water samples

So as to evaluate the performance of the method: $\text{UV/Fe}_3\text{O}_4\text{-WO}_3\text{-APTES}$ for removing the pesticide from a real water sample, 20 mg.L^{-1} of diazinon was added to a real water sample from the drinking water distribution system in Rasht City, Iran. Table 4 shows a breakdown of the properties of the real water. Since real water consists of various materials like sulphate, chloride, carbonate, bicarbonate, nitrate and nitrite, a decrease in photodegradation of the pesticide is expected (see Figure 14). Active sites on the surface of $\text{Fe}_3\text{O}_4\text{-WO}_3\text{-APTES}$ can be blocked by these ions, which may deactivate the catalysts for diazinon and intermediates [30]. Although the created radical anions have oxidation properties, they are considered as weak oxidants as compared with hydroxyl radicals. In comparison with distilled water, lower removal efficiency was seen in diazinon photodegradation; the reason for this may be because of carbonate and bicarbonate ions in real water increasing the level of pH. In the presence of $\text{Fe}_3\text{O}_4\text{-WO}_3\text{-APTES}$, the pH of the real water comprised the pesticide declined from 7.9 to 6.8, probably due to CO_2 formation. But the specific conductivity of the solution improved from 0.9 to 0.99 during the process of $\text{UV/Fe}_3\text{O}_4\text{-WO}_3\text{-APTES}$ because of the photocatalytic destruction of the pesticide form inorganic ions like SO_4^{2-} , PO_4^{3-} and NO_3^- , thereby reducing the conductivity.

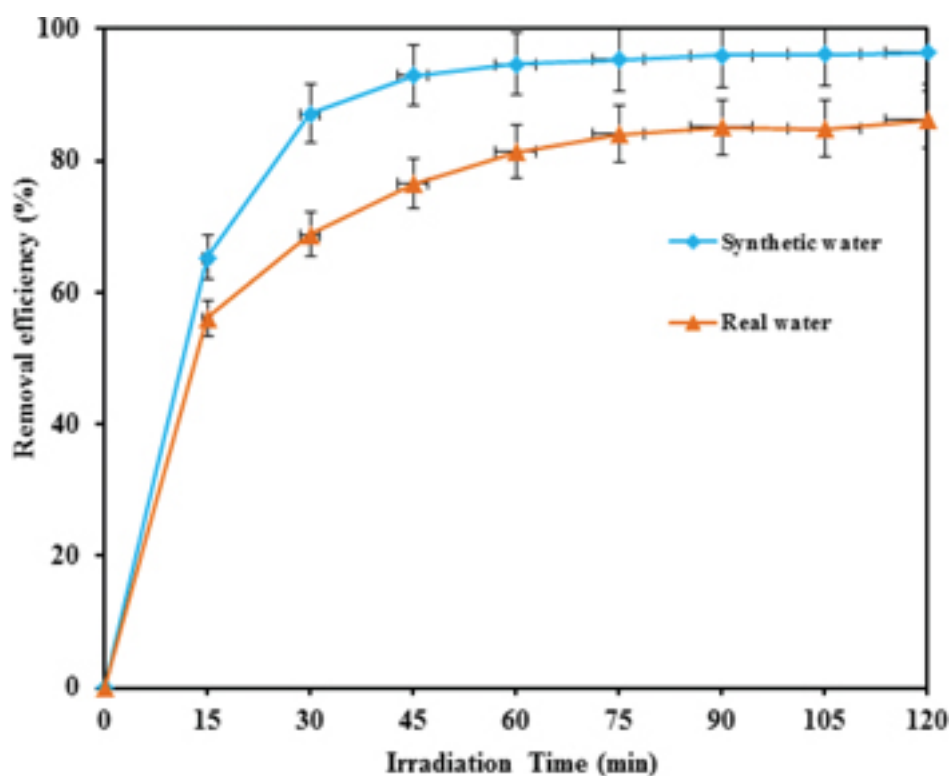


Figure 14: Investigation of the efficiency of UV/ $\text{Fe}_3\text{O}_4\text{-WO}_3\text{-APTES}$ process in removal of diazinon from real water (catalyst dosage = 0.25 g.L^{-1} , $[\text{diazinon}]_0 = 20 \text{ mg.L}^{-1}$).

Table 4: Characteristics of real water.

Parameters	Value
pH	7.9
Sulfate concentration ($\text{mg.L}^{-1} \text{SO}_4^{2-}$)	190.6
Chloride concentration ($\text{mg.L}^{-1} \text{Cl}^-$)	201
Specific conductivity (mS.cm^{-1})	0.9
Total hardness ($\text{mg.L}^{-1} \text{CaCO}_3$)	299
Calcium hardness ($\text{mg.L}^{-1} \text{CaCO}_3$)	189
Carbonate hardness ($\text{mg.L}^{-1} \text{CaCO}_3$)	100
Nitrate concentration ($\text{mg.L}^{-1} \text{NO}_3^-$)	33.3
Nitrite concentration ($\text{mg.L}^{-1} \text{NO}_2^-$)	0
Total dissolved solids (TDS) (mg.L^{-1})	776
Pesticide concentration ($\mu\text{g.L}^{-1}$)	NO*

* None observed.

4 Conclusions

In the current research, we synthesized the $\text{Fe}_3\text{O}_4\text{-WO}_3\text{-APTES}$ by means of a facile co-precipitation technique and the effects of some operating parameters: pH, $\text{Fe}_3\text{O}_4\text{-WO}_3\text{-APTES}$ nanoparticles dosage, initial diazinon concentration, oxygen and nitrogen gases, H_2O_2 concentration, and type of organic compounds were investigated. In order to characterize the nanoparticles of $\text{Fe}_3\text{O}_4\text{-WO}_3\text{-APTES}$, XRD, FT-IR, SEM, EDX, VSM and pH_{pzc} techniques were applied. Among all processes used in this study, the highest removal efficiency was achieved by the UV/ $\text{Fe}_3\text{O}_4\text{-WO}_3\text{-APTES}$ process at pH 7. The photocatalytic destruction of the pesticide increased with raising the dose of the nanocatalyst up to 0.25 g.L^{-1} . K_{Diazinon} and k_c were found to be $0.085 (\text{Lmg}^{-1})$ and $0.2016 (\text{mg.L}^{-1}\text{min}^{-1})$, respectively, by using the first-order kinetic assumption. In comparison with the UV/ WO_3 and UV/ Fe_3O_4 process, the UV/ $\text{Fe}_3\text{O}_4\text{-WO}_3\text{-APTES}$ processes had lower electrical energy consumption per order of magnitude. In addition, the photodegradation of diazinon declined in both purging gases of oxygen and

nitrogen and organic compounds. It should be noted that the photocatalytic activity remained unchanged even after five successive cycles. Approximately 86.17 % of diazinon in a real water sample was removed after 120 min under the optimal circumstances.

Acknowledgment

This paper is issued from an integrated research of IR.GUMS.REC.1395.170 as a project number MS student of Kobra Ayagh. Financial support was provided by Guilan University of Medical Sciences, Rasht, Iran.

None observed.

References

- [1] Abraham J, Silambarasan S, Logeswari P. *J Taiwan Inst Chem Eng.* 2014;45:2590–2596.
- [2] Affam AC, Chaudhuri M. *J Environ Manage.* 2013;130:160–165.
- [3] Ahmed S, Rasul MG, Brown R, Hashib MA. *J Environ Manage.* 2011;92:311–330.
- [4] Alalm MG, Tawfik A, Ookawara S. *J Water Eng.* 2015;8:55–63.
- [5] El-Dib MA, Aly OA. *Water Res.* 1977;11:611–616.
- [6] Karimi H, Rahimpour A, Shirzad Kebria MR. *Desalin Water Treat.* 2016;57:1–11.
- [7] Chatterjee S, Das SK, Chakravarty R, Chakrabarti A, Ghosh S, Guha AK. *J Hazard Mater.* 2010;174:47–53.
- [8] Jonidi-Jafari A, Shirzad-Siboni M, Yang J-K, Naimi-Joubani M, Farrokhi M. *J Taiwan Inst Chem Eng.* 2015;50:100–107.
- [9] Kalantary RR, Dadban Shahamat Y, Farzadkia M, Esrafil A, Asgharnia H. *Desalin Water Treat.* 2015;55:555–563.
- [10] Shirzad Siboni M, Samadi MT, Yang JK, Lee SM. *Environ Technol.* 2011;32:1573–1579.
- [11] Shirzad-Siboni M, Samarghandi M, Yang J-K, Lee S-M. *J Adv Oxid Technol.* 2011;14:302–307.
- [12] Andreato R, Caprio V, Insola A, Marotta R. *Catal Today.* 1999;53:51–59.
- [13] Mohagheghian A, Karimi S-A, Yang J-K, Shirzad-Siboni M. *Desalin Water Treat.* 2016;57:8262–8269.
- [14] Nakaoka Y, Katsumata H, Kaneco S, Suzuki T, Ohta K. *Desalin Water Treat.* 2010;13:427–436.
- [15] Real FJ, Benitez FJ, Acero JL, Gonzalez M. *J Chem Technol Biotechnol.* 2007;82:566–574.
- [16] Arai T, Yanagida M, Konishi Y, Iwasaki Y, Sugihara H, Sayama K. *J Phys Chem C.* 2007;111:7574–7577.
- [17] Chen D, Gao L, Yasumori A, Kuroda K, Sugahara Y. *Small.* 2008;4:1813–1822.
- [18] Adhikari S, Sarkar D, Madras G. *RSC Adv.* 2015;5:11895–11904.
- [19] Luo J, Yartym J, Hepel M. *J New Mat Elect Syst.* 2002;5:315–321.
- [20] Seddigi ZS. *Bull Environ Contam Toxicol.* 2010;84:564–567.
- [21] Xi G, Yue B, Cao J, Ye J. *Chem Eur J.* 2011;17:5145–5154.
- [22] Kurtan U, Baykal A. *Mater Res Bull.* 2014;60:79–87.
- [23] Can K, Ozmen M, Ersoz M. *Colloids Surf B.* 2009;71:154–159.
- [24] Shirzad-Siboni M, Khataee A, Vahid B, Joo SW. *Sci Adv Mat.* 2015;7:806–814.
- [25] Mohagheghian A, Vahidi-Kolur R, Pourmohseni M, Yang J-K, Shirzad-Siboni M. *Water Air Soil Pollut.* 2015;226:1–16.
- [26] Chen D, Ye J. *Adv Funct Mater.* 2008;18:1922–1928.
- [27] Horwitz W. *Standard Methods for the Examination of Water and Wastewater*, 20th ed. Washington, DC: APHA, 2000.
- [28] Rasoulifard MH, Akrami M, Eskandarian MR. *J Taiwan Inst Chem Eng.* 2015;57:77–90.
- [29] Salarian A-A, Hami Z, Mirzaie N, Mohseni SM, Asadi A, Bahrami H, et al. *J Mol Liq.* 2016;220:183–191.
- [30] Daneshvar N, Aber S, Seyed Dorraji MS, Khataee AR, Rasoulifard MH. *Sep Purif Technol.* 2007;58:91–98.
- [31] Daneshvar N, Salari D, Khataee AR. *J Photochem Photobiol.* 2003;157:111–116.
- [32] Farrokhi M, Hosseini S-C, Yang J-K, Shirzad-Siboni M. *Water Air Soil Pollut.* 2014;225:1–12.
- [33] Klayrri R, Tubchareon T, Praserttham P. *J Ind Eng Chem.* 2017;45:229–236.
- [34] Ku Y, Chang J-L, Shen Y-S, Lin S-Y. *Water Res.* 1998;32:1957–1963.
- [35] Shemer H, Linden KG. *J Hazard Mater.* 2006;136:553–559.
- [36] Shirzad-Siboni M, Jonidi-Jafari A, Farzadkia M, Esrafil A, Gholami M. *J Environ Manage.* 2017;186:1–11.
- [37] Gunther FA, Ott DE, Ittig M. *Bull Environ Contam Toxicol.* 1970;5:87–94.
- [38] Kouloumbos VN, Tsipi DF, Hiskia AE, Nikolic D, Van Breemen RB. *J Am Soc Mass Spectrom.* 2003;14:803–817.
- [39] Kalantary RR, Shahamat YD, Farzadkia M, Esrafil A, Asgharnia H. *Eur J Exp Biol.* 2014;4:186–194.
- [40] Hossaini H, Moussavi G, Farrokhi M. *Water Res.* 2014;59:130–144.
- [41] Sakkas VA, Dimou A, Pitarakis K, Mantis G, Albanis T. *Environ Chem Lett.* 2005;3:57–61.